

Flight Procedure and Community Noise Modeling of Advanced Air Mobility Flight Vehicles

Nathan Yeung^{*}, Jessica De la Cruz^{*}, Victoria Pellerito^{*}, Melissa Lepe^{*} and Jacqueline Huynh[†]
University of California Irvine, 4200 Engineering Gateway, Irvine, CA, 92617, USA

Z. Juju Wang[‡] and R. John Hansman[§]
Massachusetts Institute of Technology, 77 Massachusetts Ave., Cambridge, MA, 02139, USA

This paper describes a preliminary methodology to model the noise of varied operating procedures for Advanced Air Mobility (AAM) vehicles. Many AAM configurations have been proposed in industry, such as tilt-rotor vertical takeoff and landing vehicles, lift plus cruise vertical takeoff and landing vehicles, or short takeoff and landing vehicles, which vary in both architecture and the operational flight procedures they are capable of flying. These variations present unique noise sources that must be modeled at both the component and procedural level to estimate the overall community noise impact. Such noise sources will affect the operational factors that are most significant contributors to ground sound levels. The presented framework models community noise of various AAM vehicles and flight procedures. Given an operation definition, a force-balance kinematics profile incorporating aircraft type, performance characteristics, and rotor geometry, is used to determine the aircraft state vector along the trajectory. This state vector is used to obtain rotor, airframe, and interaction source noise utilizing methods from the NASA Aircraft NOise Prediction Program 2. Utilization of this framework in the prediction of community noise for example blown-flap short takeoff and landing, as well as lift plus cruise and tilt-rotor vertical takeoff and landing aircraft flying at various flight procedures for potential low noise operations is presented.

I. Nomenclature

| | | |
|-----------|---|---|
| a | = | Acceleration |
| AAM | = | Advanced Air Mobility |
| $ANOPP$ | = | Aircraft NOise Prediction Program |
| dB | = | Decibels |
| ft | = | Feet |
| $KSMO$ | = | Santa Monica Airport |
| L_{AE} | = | Sound Exposure Level |
| LPC | = | Lift Plus Cruise |
| M_{tip} | = | Rotor Tip Mach Number |
| nm | = | Nautical Miles |
| $OASPL$ | = | Overall A-weighted Sound Pressure Level |
| R | = | Rotor Radius |
| RPM | = | Revolutions per Minute |
| $STOL$ | = | Short Takeoff and Landing |
| T | = | Thrust |

^{*}Graduate Student, Department of Mechanical and Aerospace Engineering, AIAA Student Member

[†]Assistant Professor, Department of Mechanical and Aerospace Engineering, AIAA Member

[‡]Graduate Student, Department of Aeronautics and Astronautics, AIAA Student Member

[§]Professor, Department of Aeronautics and Astronautics, AIAA Fellow.

| | | |
|-----------------|---|---|
| V | = | Velocity |
| V_j | = | Rotor Jet Velocity |
| V_∞ | = | Freestream Velocity |
| $VTOL$ | = | Vertical Takeoff and Landing |
| α | = | Rotor Angle of Attack for Tilt-Rotor VTOL Vehicle |
| β_{pitch} | = | Rotor Pitch Angle |
| δ_f | = | Flap Deflection |
| γ | = | Flight Path Angle |
| $()_i$ | = | Per Segment |
| $()_x$ | = | x-Direction |
| $()_y$ | = | y-Direction |
| $()^*$ | = | Per Rotor |

II. Introduction

ADVANCED Air Mobility (AAM) has the potential to dramatically alter the number and types of flight missions available in the national airspace. With the capability of performing inter-city missions that could not otherwise be done with current air travel methods, hundreds of companies have begun to invest in the development of such vehicles [1]. As more AAM vehicles are developed, the ability to assess and mitigate their noise impacts will become pertinent, particularly as noise remains a major constraint in the implementation of AAM [2].

Various vehicle types are currently under consideration in their feasibility to perform AAM operations, including but not limited to blown-flap short takeoff and landing (Blown-Flap STOL) vehicles, tilt-rotor vertical takeoff and landing (Tilt-Rotor VTOL) vehicles, and lift plus cruise vertical takeoff and landing (LPC-VTOL) vehicles, as diagrammed in Fig. 1. Each AAM vehicle may feature unique sources of noise stemming from varied configurations with different numbers of rotors and their placements, which may interact with each other and with the airframe. In addition, the standard flight operations of different vehicle types may vary. Therefore, to determine overall community noise impacts of these vehicles, a noise assessment must consider both flight procedures and source components in various operating conditions [3].

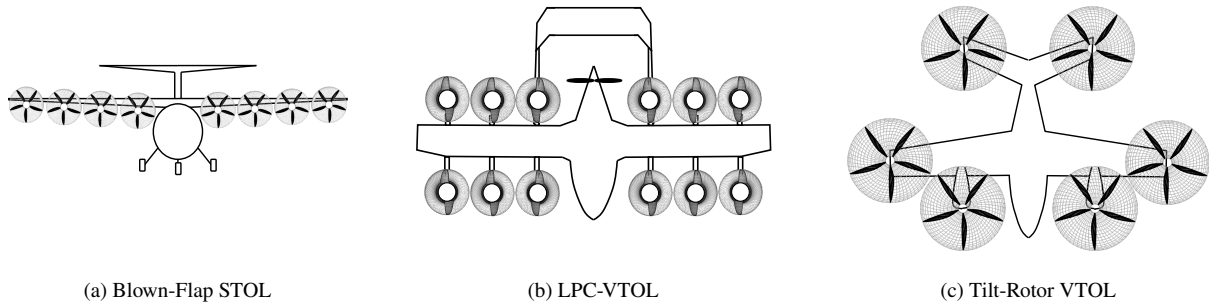


Fig. 1 Example AAM vehicle types

This paper demonstrates a preliminary community noise modeling methodology for a variety of AAM types and flight operations. This is accomplished by analyzing three representative vehicle types and their potential noise sources through standard departure and arrival procedures. The examples selected for this analysis include a 9 passenger Blown-Flap STOL vehicle, a 2 passenger LPC-VTOL vehicle, and a 4 passenger Tilt-Rotor VTOL vehicle. A noise analysis methodology is developed to estimate the flight performance and resulting noise impacts at different operating states among approach and departure procedures for each of the representative AAM vehicles. The full modeling methodology is exercised through the community noise assessment of representative departure and arrival procedures for each vehicle type.

III. AAM Noise Modeling Framework

The community noise modeling approach for AAM vehicles is presented in Fig. 2. The initial inputs to the modeling framework consists of an operation definition such as a short takeoff followed by steep climb during departure, or a vertical takeoff to a cruise altitude followed by a transition to cruise, along with the aircraft type (Tilt-Rotor VTOL, Blown-Flap STOL, or LPC-VTOL) and characteristics. These inputs are used to generate a state vector of the aircraft along a flight profile developed on a segment-by-segment basis. The state vector is generated using a force-balance-kinematics model as constrained by the vehicle performance characteristics from the Aircraft Performance Module. In the Aircraft Performance Module, the aircraft characteristics such as wing shape, weight, rotor placement and design conditions are utilized to design representative rotors according to the vehicle performance specifications. The details of these processes are described in further detail in sections III.A and III.B. The elements of the aircraft state vector along the trajectory become inputs to the Source Noise Module, enabling an evaluation of the component noise levels for varying aircraft configurations, flight trajectories, and operational settings.

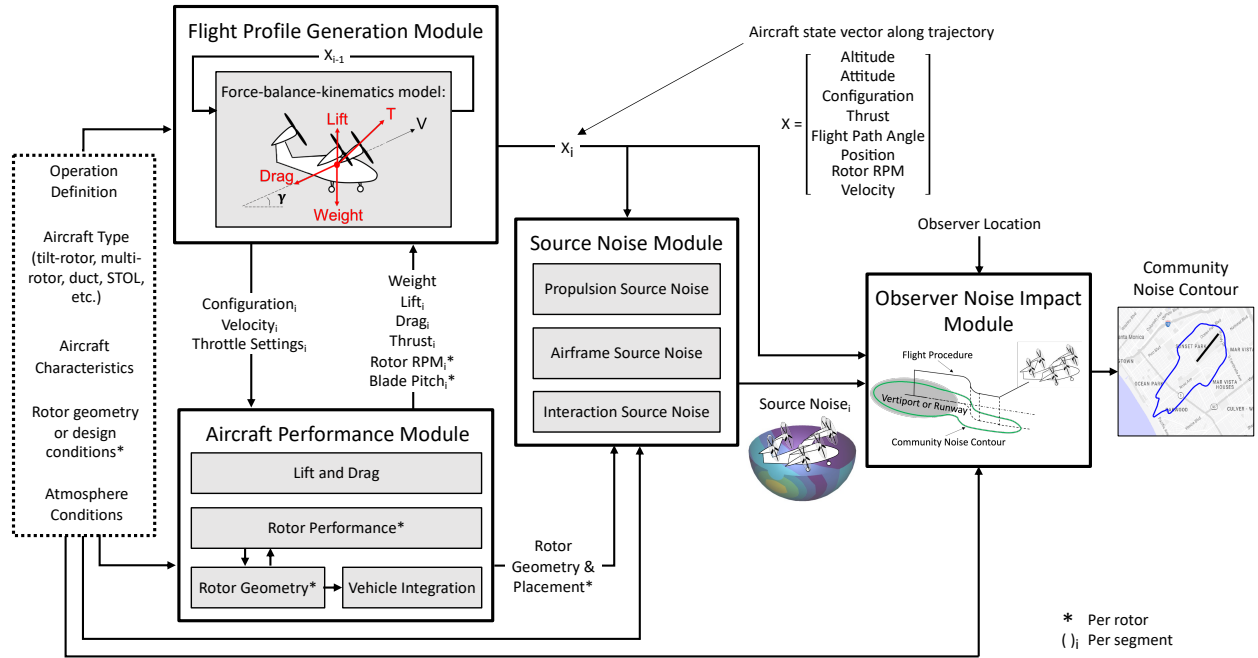


Fig. 2 AAM noise modeling framework

Methods from the NASA Aircraft Noise Prediction Program (ANOPP2) [4] are incorporated within the Source Noise Module to determine the noise levels over a hemisphere at significant transition segments of the flight procedure and is described in additional detail in section III.C. A similar model to the one shown in Fig. 2 utilizing modules from ANOPP has already been developed by the authors to evaluate community noise of tube and wing aircraft around airports [3]. Given the hemispherical source noise around the vehicle during each flight segment, the noise is propagated from the aircraft source to the ground at the desired observer locations, such as a population grid surrounding an airport, given assumed atmospheric conditions within the Observer Noise Impact Module. As such, the presented framework enables the assessment of community noise levels for varied AAM types and operations.

A. Flight Profile Generation Module

The AAM flight procedure modeling implemented here follows the methodology from [5] to determine the aircraft state vector shown Fig. 2. This state vector is necessary for determining the source noise of each segment and producing the observer noise impact of the flight procedure as described in section III.C. Provided an operation definition, such as a vertical takeoff to a given altitude followed by a high power climb, along with an AAM vehicle type and corresponding performance characteristics, the flight profile is constructed on a segment by segment basis by

determining the aerodynamic loads that influence the inertial characteristics of the AAM vehicle type. The mentioned loads are dependent on the geometry and propulsive system arrangement of a particular vehicle architecture. The governing physics of an arbitrary AAM vehicle is summarized by a point mass model with component level equations provided in eq. 1 and 2. The flight procedure is segmented according to significant changes that will impact source noise, such as changes in thrust, velocity, or vehicle configuration. The directional components for aerodynamic loads are identified for the example vehicles in sections IV, V, and VI.

$$T_x - Drag_x - Lift_x = ma_x \quad (1)$$

$$T_y - Drag_y + Lift_y - Weight = ma_y \quad (2)$$

B. Aircraft Performance Module

The methodology to model the aerodynamic forces of AAM vehicles described in Fig. 2 is expanded in Fig. 3, which shows the aircraft performance module. Given the aircraft characteristics, aircraft type and rotor geometry or design condition, the aircraft performance module determines the magnitude of the vehicle aerodynamic forces, as well as the RPM necessary to build the flight physics in the Flight Profile Generation Module. It also determines the geometry and placement of each rotor on the vehicle necessary for source noise modeling.

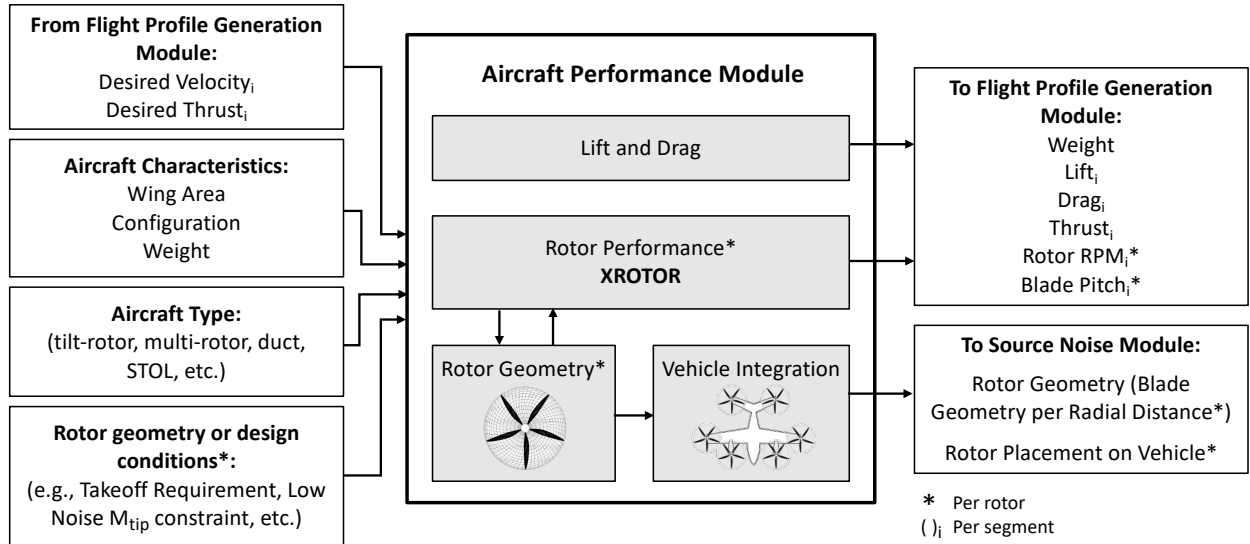


Fig. 3 Aircraft Performance Module within the AAM noise modeling framework

Within the Aircraft Performance Module, the thrust, lift and drag are obtained for each flight segment while the vehicle weight is assumed to be constant throughout the flight procedure. The lift and drag are determined with equations provided in eq. 1 and 2, given the previously mentioned aircraft characteristics such as wing area, configuration and weight, as well as the aircraft type. Lift coefficient are determined as needed to balance the vertical aerodynamic loads per segment. The total coefficient of drag is separated into the zero-lift and the induced drag coefficient. The zero-lift coefficient of drag in cruise is obtained from [5] and is modified for vehicles with altered configuration settings. The induced drag was determined from the given aircraft geometry, desired velocity, and segment lift coefficient.

The flight segment rotor performance conditions, such as thrust, RPM, and pitch angle are obtained by modeling performance conditions at the segment desired velocity and thrust condition (or desired RPM) for the rotor in the blade element momentum rotor theory design tool, XROTOR. The performance is modeled for either a given input rotor geometry if available or a representative rotor designed uniquely for each vehicle architecture design condition. As described in Fig. 3. A design operating condition (such as a takeoff requirement) for the specified AAM mission requirements is used to design a rotor geometry in XROTOR. Such design condition is dependent on whether the AAM consists of a designed fixed or variable pitch rotor. For a variable pitch rotor, the operating point is selected from the

performance takeoff and cruise conditions since the methodology for rotor design gives equal importance to achieving a good takeoff and climb angle, as well as, high cruise speeds. As suggested by Weick, a rotor with a design point about half-way in between the two extremes results in a rotor with good high-speed cruise performance while resulting in a takeoff roll nearly as short as the best takeoff rotor [6]. Thus for a variable pitch rotor, a midpoint magnitude of speed, thrust and RPM between the low and high-speed vehicle operative performance extremes is used for sizing. For a fixed-pitch rotor, the operating design point however is selected as either from the takeoff or cruising performance conditions. For any vehicle, after a designed rotor geometry with a preliminary diameter, blade count, blade twist and chord per radial station, and the design point operating thrust, velocity and RPM is determined, the design point is shifted to match the unique performance characteristic of each AAM vehicle with a minimum rotor diameter to reduce M_{tip} , and thus reduce noise, within the design constraints.

Rotor performance on each flight segment is inputted into the Flight Profile Generation Module to build the flight dynamics. The rotor geometry output process is simultaneously repeated to position all rotors configuration for vehicle integration. Such rotor geometry and respective vehicle position is outputted into the Source Noise Module to model the noise per segment as described in the following section.

C. AAM Noise Modeling

The methodology to model source noise hemispheres of AAM vehicles described in Fig. 2 is expanded in Fig. 4. Noise sources are assumed to be divided into rotor source noise, airframe source noise, and interaction effects, which vary depending on the AAM vehicle type, configuration, and rotor geometry. The radius of a noise source hemisphere was sized with the purpose of obtaining far-field noise values on the hemisphere surface. A distance away from closest rotor to the edge of the hemisphere of five times the diameter that rotor for each vehicle type was assumed based on recommendations from [7].

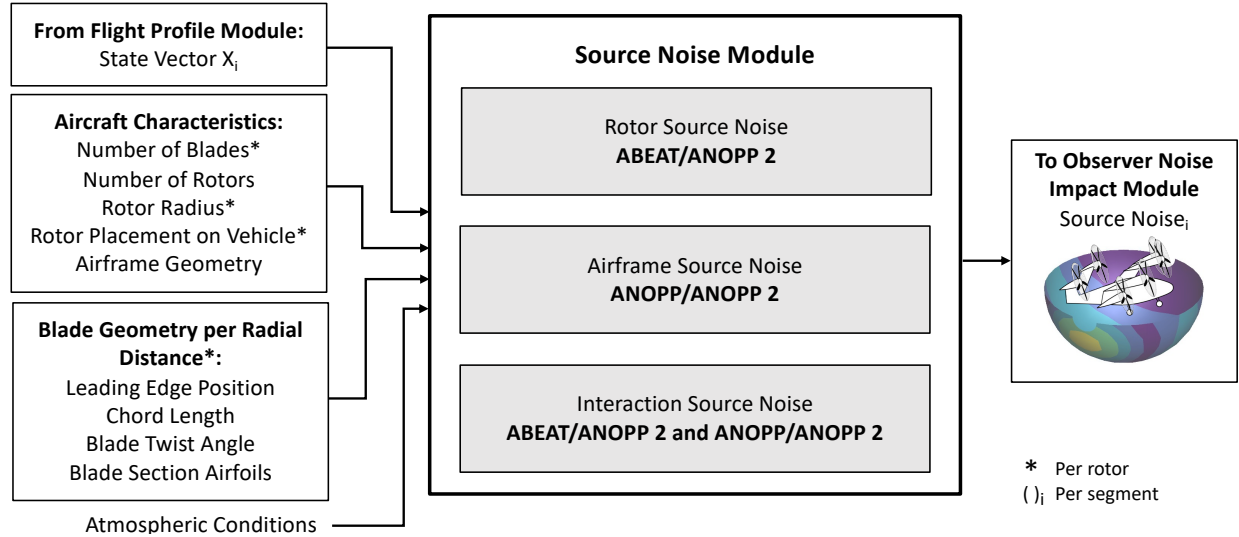


Fig. 4 Source component noise module within AAM noise modeling framework

Propulsion Noise: For the vehicle types described in Fig. 1, rotor noise is assumed to be due to tonal and broadband components of distributed propulsion. ANOPP2's Blade Element Acoustic Tool (ABEAT) [8] is used to model rotor tonal and broadband noise. Rotor discrete loading and thickness noise is modeled using Farassat methods from the inputted blade geometry, such as blade chord length and twist per radial section, and aerodynamic loads from blade-element-momentum theory. Rotor blade broadband self-noise is modeled from semi-empirical methods [9]. The state vector from the Flight Profile Generation Module, as described in section III.A, defines the rotor RPM and the vehicle forward velocity necessary to determine the blade loads for this method.

Airframe Noise: Airframe noise is assumed to consist of classic aircraft components such as the wing and tail trailing edge boundary layer interaction noise, high lift device noise, and landing gear noise. Trailing edge noise is computed with the Fink method [10] and high lift devices and landing gear with the Guo methods [11][12] implemented

in ANOPP. The airframe noise methods require airframe geometry and scale with the incoming flow velocity at each component.

Interaction Noise: Interaction noise sources include both rotor-rotor interaction sources and airframe-rotor interaction sources and are modeled using ABEAT and ANOPP methods in the preliminary framework. Interaction sources must be defined for each vehicle type, and can include sources such as rotor-aerodynamic surface/airframe interaction noise, tonal inter-rotor constructive/destructive interference noise, rotor-wake interaction noise from multiple rotors in close proximity to each other, rotor-wake fuselage interactions, and blade-vortex interactions.

For example, for a Blown-Flap STOL vehicle that achieves short takeoff and landing distances via blown lift as described in [13] a rotor wake-aerodynamic surface interaction noise source includes rotor wake-flap and rotor wake-wing trailing edge interaction noise. This interaction noise source is assumed to be a result of the increased local flow velocity from the rotor wake interacting with the wing as well as flaps at high deflection angles. In this case, the rotor wake-flap and rotor wake-trailing edge interaction noise is approximated using the Guo flap side edge noise and Fink trailing edge noise models as described in [14], with the estimated rotor wake velocity in different operations. Constructive/destructive interference noise is determined in ABEAT for aircraft cases with multiple rotors. Certain configurations with multiple rotors for and aft of each other may experience rotor-wake interaction noise. While not included for the examples shown in this paper, rotor-wake interaction noise is modeled as classic rotor noise with disturbed inflow based on the inflow fluctuation velocities from a forward rotor implemented in ABEAT to showcase interaction with a rear rotor. Additional sources such as rotor-wake fuselage interactions and blade-vortex interactions will be included in future iterations of the framework.

The noise for each component is modeled as a source noise hemisphere as a function of frequency and directivity. Given modeled rotor, airframe, and interaction noise sources at each segment, the noise is propagated using ANOPP2 to the observers within the Observer Noise Impact Module based on atmospheric conditions and attenuation. The final output is represented in metrics such as Overall A-weighted sound pressure level (OASPL) and Sound Exposure Level (L_{AE}).

IV. Community Noise Modeling Demonstration of a Blown-Flap STOL Vehicle

In this section, example departure and arrival flight operations and resulting community noise characteristics of a representative 9 passenger Blown-Flap STOL vehicle is presented.

A. Vehicle Characteristics

The Blown-Flap STOL vehicle used for analysis is assumed to operate similar to a conventional fixed wing aircraft and is presented in Fig. 5a. In order to achieve short takeoff and landing field lengths, the Blown-Flap STOP vehicle utilizes distributed propulsion and blown flap technology as described in [15]. The jet produced by the rotor wake, V_j , as noted in Fig. 6, increases the flow velocity at the flap, which provides higher C_L values.

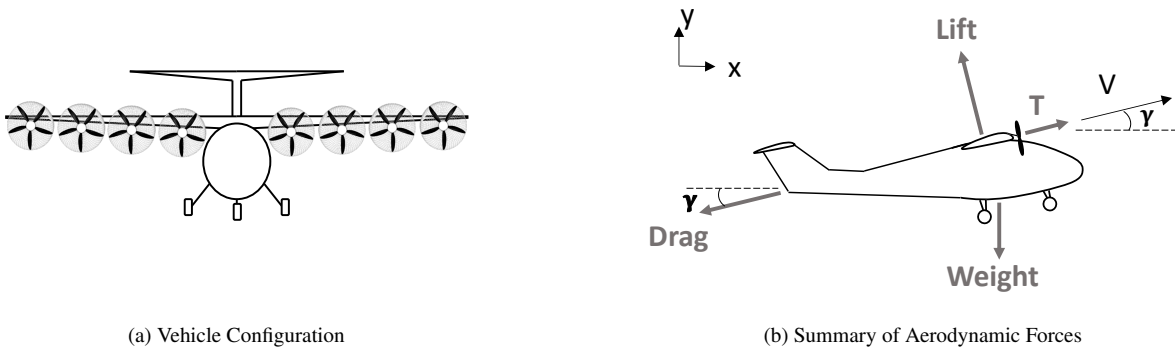


Fig. 5 Vehicle Summary for Blown-Flap Short Takeoff and Landing (STOL)

Blown lift also induces a unique source of drag from the blowing jet of the rotor wake. The drag due to blowing is determined via the momentum theory of jet contraction, following the analysis in [14]. Such coefficient is added to the total drag buildup in this analysis. The thrust direction is otherwise assumed to follow the direction of flight, with flight

path angle denoted as γ shown in Fig. 5. The aerodynamic forces summarized in the figure are calculated according to the methods described in Section III.B and used to construct the flight profile according to eq. 1 and 2 as described in section III.A.

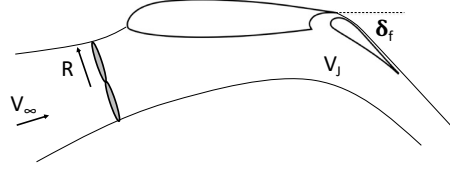


Fig. 6 Rotor wake interaction with the flap in Blown-Flap STOL aircraft

A description of key vehicle properties used as inputs to model the flight performance, rotor blade geometry, and noise are described in Table 1, with aircraft characteristics, takeoff distance, and cruise speed used in the rotor design, and the known rotor geometries with the exception of the rotor diameter, taken from [5]. Additional flap geometries and performance were taken from the sub-scale STOL demonstrator from [13], scaled to full-scale. The design takeoff thrust and cruise thrust per rotor were determined as described in section III.A based on the design takeoff distance and speed, and design cruise speed, respectively. The vehicle was assumed to have a 150 *ft* takeoff field length, as indicated in [5]. A lift coefficient, C_L , of 6 was assumed during the departure, yielding a takeoff speed of 38 knots that is used to design the rotors used for the noise analysis.

Table 1 Blown-Flap STOL vehicle properties, referenced from [5] and [13], used for example noise analyses

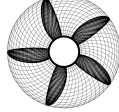
| | | |
|--|---------------------------------------|----------------------|
| Aircraft Characteristics | Weight (lbs) | 6000 |
| | Span (ft) | 43.7 |
| | Aspect Ratio | 7.9 |
| | Range (nmi) | 348 |
| | Number of Passengers | 9 |
| Known Rotor Geometry | Rotor Diameter (ft) | 2.7** |
| | Number of Rotors | 8 |
| | Number of Blades per Rotor | 5 |
| | Hub Percent of Rotor Diameter (%) | 25 |
| Takeoff and Cruise Operating Points used for Rotor Design | Takeoff Distance (ft) | 150 |
| | Design Takeoff Thrust per Rotor (lb)* | 229 |
| | Design Takeoff Speed (knots)* | 38 |
| | Design Cruise Thrust per Rotor (lb)* | 106 |
| Additional Considerations | Flap Settings | 35° Flaps on Takeoff |
| | | 65° Flaps on Landing |

*Determined from desired takeoff and cruise performance

**Diameter changed from [5] to lower tip Mach number

To obtain the rotor geometry per blade section needed for the noise analysis, the rotors for this vehicle were designed with the methodology described in section III.B for a variable pitch rotor. A preliminary design point was used between the thrust required for the 150 *ft*² takeoff ground roll and the design cruise thrust obtained at a speed of 152 knots. The Blown-Flap STOL rotor uniquely had to produce higher thrust magnitudes at lower speeds while having optimum efficiency during cruise. The midpoint design velocity was shifted to a lower speed to assure low-speed performance while simultaneously optimizing for cruise efficiency. In addition, rotor diameter was reduced to minimize M_{tip} to 0.392 and lower noise as explained in section III.B. This results in a maximum RPM of 4000 for maximum takeoff thrust conditions with rotor design condition of a slow end of climb. A summary of the rotor properties is given in Table 2.

Table 2 Modeled Blown-Flap STOL rotor properties used for example noise analyses

| Design Condition | Slow end of climb |
|--|--|
| Thrust per rotor at Design Condition (N) | 1020 |
| Velocity at Design Condition (m/s) | 20 |
| Power per rotor at Design Condition (kW) | 48 |
| RPM at Design Condition | 3200 |
| M_{tip} at Design Condition | 0.392 |
| Max RPM | 4000 |
| Rotor characteristics | Variable pitch |
| Rotor image |  |

B. Example Noise Analysis of a Maximum RPM Blown-Flap STOL Departure Compared to a Maximum RPM Departure with Cutback

Given the vehicle and rotor properties from Tables 1 and 2, noise analysis was performed on example departure and arrival procedures to demonstrate the methodology outlined in section III.

The first example departure procedure is a maximum 4000 RPM, $150 ft^2$ super short field length departure at a flap angle of δ_f of 35° . Once rotated, the aircraft maintains a constant velocity of 38 knots. A resultant climb angle of 13° was determined for this condition based on the flight vehicle characteristics. In comparison, a second example departure procedure was modeled, assuming the same initial conditions but with the inclusion of a cutback to 3200 RPM and a resultant decrease in the climb angle. In addition, the velocity of the rotor wakes impinging on the flaps was determined using from actuator disk theory as described in [14]. The resultant procedures are shown in Fig. 7 a and b.

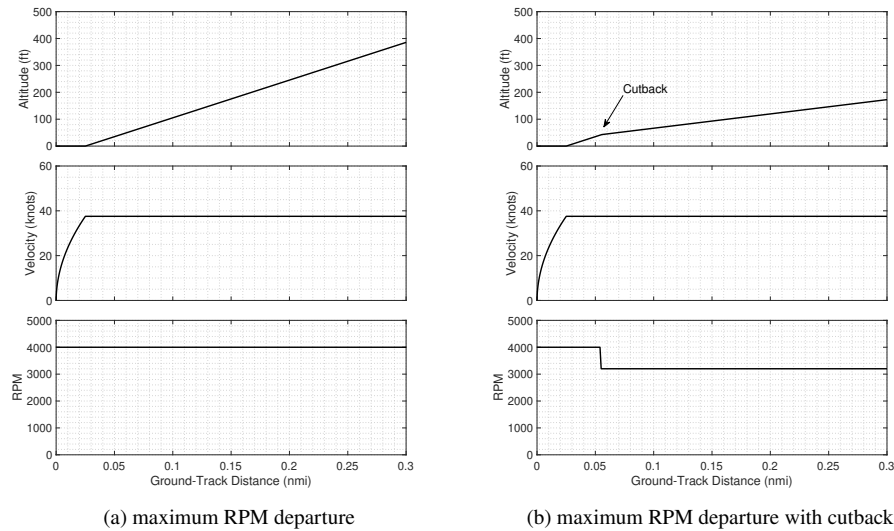
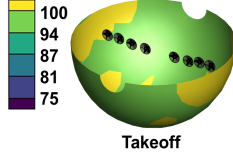
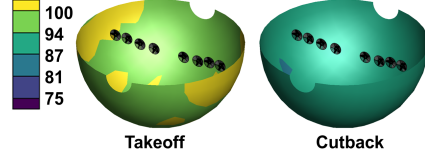


Fig. 7 Example modeled departure procedures for a 9 passenger Blown-Flap STOL aircraft

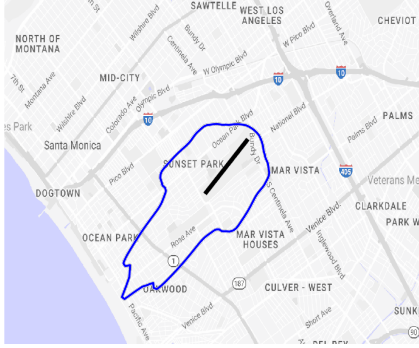
Given the inputs described above, noise source hemispheres were modeled using the source noise module along the flight trajectory, as shown in Fig. 8 a and b. A single takeoff hemisphere was adequate to model the first departure, while the second departure was modeled with the takeoff hemisphere followed by a hemisphere for the cutback condition after the cutback location. These noise hemispheres were propagated to the ground in the Observer Noise Impact Module from Fig. 2. The L_{AE} noise at the 80 dB level are shown in Fig. 8 c and d, overlaid at Santa Monica Airport (KSMO) for demonstration.



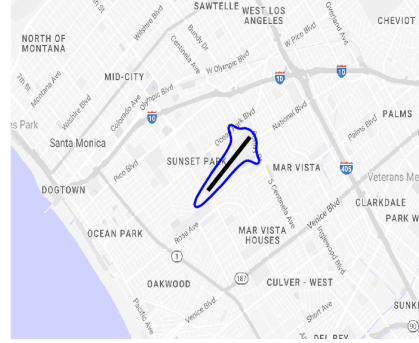
(a) A-Weighted OASPL (dBA) noise hemispheres for maximum RPM departure



(b) A-Weighted OASPL (dBA) noise hemispheres for maximum RPM departure with cutback



(c) 80 dB L_{AE} contour for maximum RPM departure



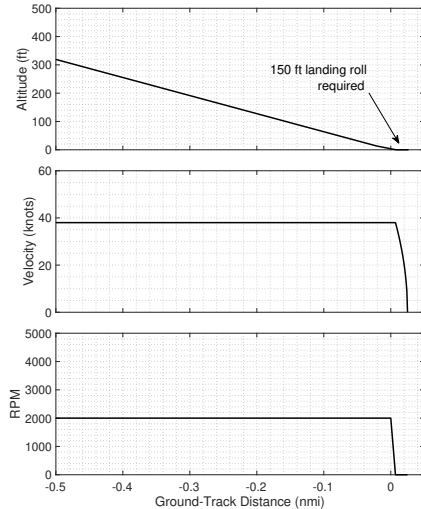
(d) 80 dB L_{AE} contour for maximum RPM departure with cutback

Fig. 8 Modeled noise hemispheres and L_{AE} (dB) contours overlaid at KSMO of example departure procedures for a 9 passenger Blown-Flap STOL aircraft

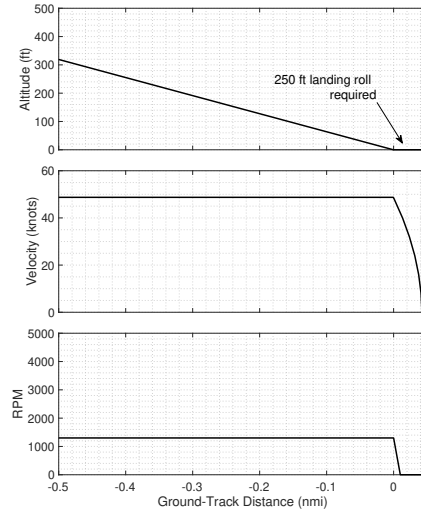
The example demonstrated in Fig. 7 and 8 shows a significant decrease in the total noise levels with rotor RPM for the cutback procedure compared to the maximum RPM procedure. This is despite the reduction in climb gradient, indicating a sensitivity to rotor RPM in this example vehicle design for potential low noise departure procedures.

C. Example Noise Analysis of -6° Descent Blown-Flap STOL Arrivals at Different Descent Speeds

The example arrival operation definitions for this vehicle are -6° continuous descent approaches at approach speeds of 38 and 48 knots and a flap angle of δ_f of 65° , and are shown in Fig. 9 a and b.



(a) -6° descent 38 knots arrival



(b) -6° descent 48 knots arrival

Fig. 9 Example modeled approach procedures for a 9 passenger Blown-Flap STOL aircraft

The resultant thrust and RPMs to maintain these conditions were determined from the methodology described in

section III.B. In addition, the velocity of the rotor wakes impinging on the flaps was determined using from actuator disk theory as described in [14]. As can be seen in the modeled procedures, the 48 knots arrival requires a longer landing roll distance.

Given the inputs described above, source noise hemispheres were modeled using the source noise module along the flight trajectory, as shown in Fig. 10 a and b. Since constant conditions were maintained for both procedures, a single hemisphere was modeled for each case. These noise hemispheres were propagated to the ground in the Observer Noise Impact Module from Fig. 2. The L_{AE} noise at the 75 dB level are shown in Fig. 10 c and d, overlaid at KSMO for demonstration.

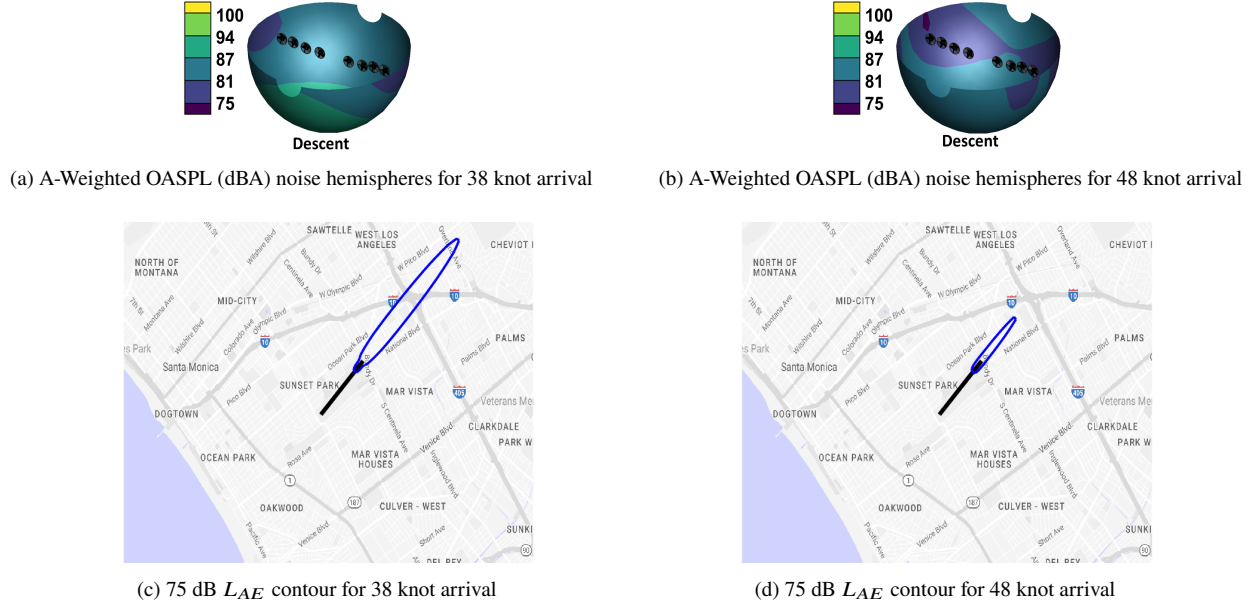


Fig. 10 Modeled noise hemispheres and L_{AE} (dB) contours overlaid at KSMO of example approach procedures for a 9 passenger Blown-Flap STOL aircraft

The examples demonstrated in Fig. 9 and 10 were dominated by the rotor wake-flap interaction noise in these low RPM, high flap angle conditions. In addition, the results show a decrease in the total noise levels for the higher velocity procedure due to the lower rotor wake velocity impinging on the flaps. This is despite the vehicle traveling at a higher freestream velocity overall, indicating a sensitivity to approach velocity in this example vehicle design for potential low noise approach procedures. The higher speed approach requires a longer landing roll distance, which would need to be considered for such procedures.

V. Community Noise Modeling Demonstration of a LPC-VTOL Vehicle

In this section, example departure and arrival flight operations and resulting community noise characteristics of a representative 2 passenger, LPC-VTOL vehicle is presented.

A. Vehicle Characteristics

The LPC-VTOL vehicle, diagramed in Fig. 11 a is assumed to operate with two independent propulsive systems that govern the dynamics for vertical and forward flight, respectively. A horizontal thrust per rotor denoted T_x is achieved from horizontal propeller(s). Likewise, a vertical thrust per rotor, denoted T_y , is obtained from vertical rotor(s). The total thrust in the corresponding directions are used to construct the flight profile according to eq.1 and 2 as described in section III.A. The inertial properties of this vehicle are obtained by assuming this fixed directionality for each rotor disk throughout the flight procedure and the vehicle is assumed to remain level during all modes of flight, as seen in Fig. 11 b.

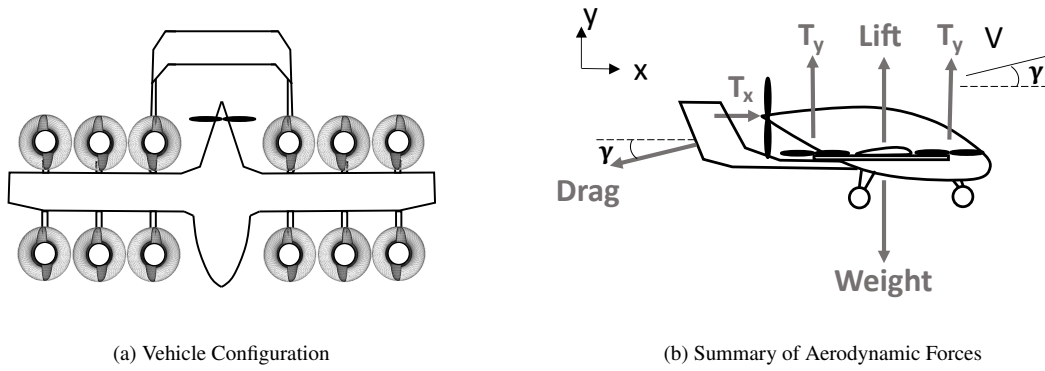


Fig. 11 Vehicle Summary for LPC-VTOL

A description of key vehicle properties used to model the flight performance characteristics, rotor blade geometry, and noise are described in Table 3, with aircraft characteristics and rotor tip and hub diameter and blade count taken from [16]. The takeoff thrust and cruise thrust per lifting and cruising rotors used in the rotor design were determined as described in section III.A based on the weight and design cruise speed, respectively. The vertical takeoff thrust magnitude is assumed to be 1.3 times the vehicle weight while the design cruise thrust was obtained from the drag at the cruise speed of a 152 knots given in Table 3. These conditions were used to determine the takeoff and cruise rotor geometries as discussed in section III.B.

Table 3 LPC-VTOL vehicle properties, referenced from [16], used for example noise analyses

| | | |
|--|-----------------------------------|--|
| Aircraft Characteristics | Weight (lbs) | 2800 |
| | Span (ft) | 36 |
| | Aspect Ratio | 12.4 |
| | Range (nmi) | 45.2 |
| | Number of Passengers | 2 |
| Known Rotor Geometry | Rotor Diameter (ft) | Lift Rotors: 4.3 Cruise Rotors: 6.6 |
| | Number of Rotors | Lift Rotors: 12 Cruise Rotors: 1 |
| | Number of Blades per Rotor | Lift Rotors: 2 Cruise Rotors: 1 |
| | Hub Percent of Rotor Diameter (%) | Lift Rotors: 30 Cruise Rotors: 20 |
| | Takeoff Distance (ft) | 0 |
| Takeoff and Cruise Operating Points used for Rotor Design | Design Takeoff Thrust per Rotor* | Lift Rotors: 303 Cruise Rotors: 0 |
| | Design Takeoff Speed (knots)** | 38 |
| | Design Cruise Thrust per Rotor* | Lift Rotors: 0 Cruise Rotors: 111 |
| | Design Cruise Speed (knots)* | 152 |

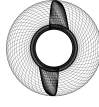
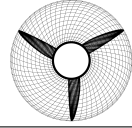
*Determined from desired takeoff and cruise performance

**Value assumed from Blown-Flap STOL vehicle example for rotor sizing

To obtain the rotor geometry per blade section needed for the noise analysis, the lift rotors and cruise rotor were

designed with the methodology described in section III.B for fixed pitch rotors. The design takeoff and cruise thrust and velocity seen in Table 4 were selected to be the design conditions for the lift and cruise rotors as previously stated. The rotor diameter was minimized for both the lift and cruise rotors to lower M_{tip} to 0.579 and 0.479 respectively. This results in an RPM of 2900 for the lift rotors and a cruise RPM of 1600 for the cruise rotor at the design conditions. A summary of the rotor properties is given in Table 4.

Table 4 LPC-VTOL rotor properties used for example noise analyses

| Rotor Type | Lifting Rotor | Cruising Rotor |
|--|--|---|
| Design Condition | Takeoff | Cruise |
| Thrust per rotor at Design Condition (N) | 1350 | 500 |
| Velocity at Design Condition (m/s) | 20 | 50 |
| Power per rotor at Design Condition (kW) | 55.4 | 28.2 |
| RPM at Design Condition | 2900 | 1600 |
| M_{tip} at Design Condition | 0.579 | 0.479 |
| Max RPM | 2900 | 1600 |
| Rotor characteristics | Fixed pitch | Fixed pitch |
| Rotor image |  |  |

B. Example Noise Analysis of a Maximum Power LPC-VTOL Departure Compared to a Maximum Power Departure with 100 ft Level Acceleration

Given the vehicle and rotor properties from Tables 3 and 4, noise analysis was performed on example departure and arrival procedures to demonstrate the methodology outlined in section III.

Presented in Fig. 12 a and b are the example departure procedures for the LPC-VTOL vehicle. The first example departure procedure is maximum power departure consisting of a 2400 RPM vertical takeoff to 100 ft followed by a

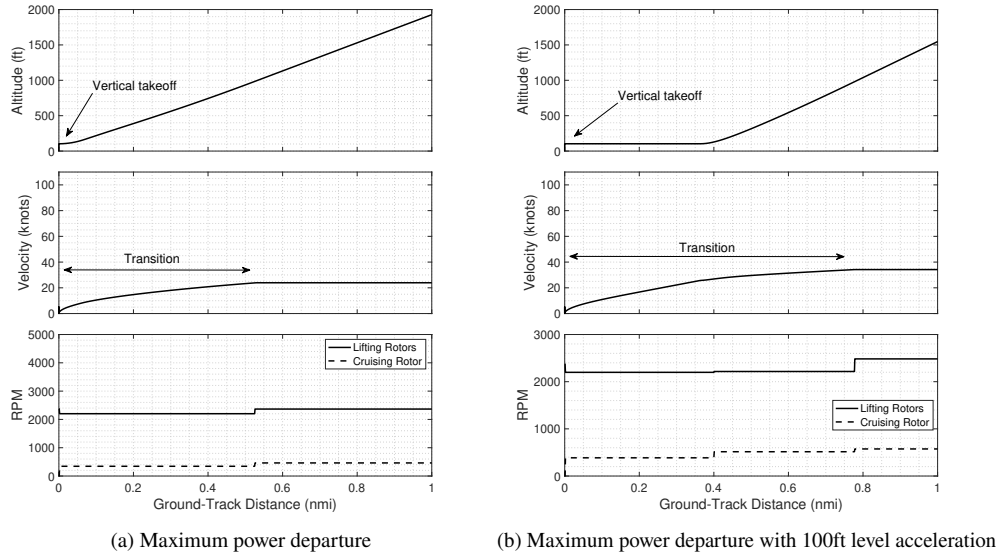
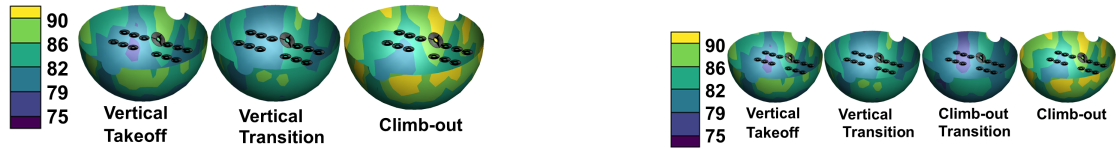


Fig. 12 Example modeled departure procedures for a 2 passenger LPC-VTOL vehicle

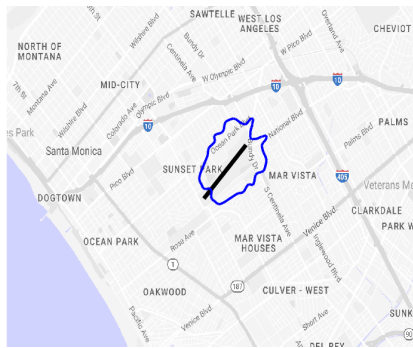
steady climb at an angle of 17° as the vehicle transitions to forward flight while accelerating to 20 knots at the end of this segment. The transition period spans just over 0.5 nm. This is compared to a level acceleration case where the vehicle increases forward airspeed but maintains 100 ft of altitude after the initial vertical takeoff. After 0.4 nm, the vehicle continues to accelerate but begins to climb at an angle of 17° . The transition period for the level acceleration case spans just under 0.8 nm reaching 35 knots at the end of this segment.

Given the inputs described above, source noise hemispheres were modeled using the source noise module along the flight trajectory. The level acceleration case required two intermediate transition hemispheres to account for the different level and climbing portions while the maximum power case was adequately represented with one transition hemisphere. Both departure cases were represented by the same vertical takeoff and cruise noise hemispheres. These noise hemispheres were propagated to the ground in the Observer Noise Impact Module from Fig. 2. The L_{AE} noise at the 80 dB level are shown in Fig. 13 c and d, overlaid at KSMO for demonstration.

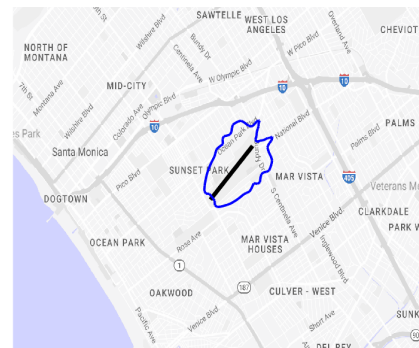


(a) A-Weighted OASPL (dBA) noise hemispheres for the maximum power departure

(b) A-Weighted OASPL (dBA) noise hemispheres for the maximum power departure with 100 ft acceleration



(c) 80 dB L_{AE} contour for the maximum power departure



(d) 80 dB L_{AE} contour for the maximum power departure with 100 ft acceleration

Fig. 13 Modeled noise hemispheres and L_{AE} (dB) contours overlaid at KSMO of example departure procedures for a 2 passenger LPC-VTOL aircraft

As shown in Fig. 13, the 100 ft level acceleration case results in elongated but narrowed noise contour compared the maximum power case with an immediate climb. Although the vehicle remains at a low altitude, its higher velocity results in a less time spent over an area. This change in contour shape is small, however, and both departure procedures maintain the same overall pattern. Since both cases were flown at maximum power, this suggests the noise of the LPC-VTOL is primarily influenced by rotor RPM rather than attenuation from flight path variations.

C. Example Noise Analysis of an LPC-VTOL Transitional Approach with Vertical Landing Compared to a Standard -3° Continuous Descent Approach

The first example LPC-VTOL arrival operation is a transitional approach at -3° with a vertical landing consisting of a decelerating transitional segment from an initial descent speed of 48 knots, in which the lifting rotors increases thrust from a cruise setting of 2000 RPM to a lifting transition mode of 2150 RPM. During this segment, the rear cruise rotor is shut off from the initial descent condition 750 RPM. Once the vehicle airspeed drops to 20 knots, the vehicle performs a fully vertical landing directly over the runway using only the lift propellers. This is compared to a standard -3° continuous descent approach, in which the LPC-VTOL maintains a 48 knots cruise velocity while descending without transitioning the lift and cruise rotor modes. The rotors are shut off when the vehicle lands and the vehicle undergoes a 400 ft landing roll to complete the approach segment.

Given the inputs described above, noise source hemispheres were modeled using the source noise module along the flight trajectory, as shown in Fig. 14 a and b. The standard approach was represented by a descent configuration noise hemisphere while the vertical landing case required the two additional transition and vertical flight noise hemispheres. These noise hemispheres were propagated to the ground in the Observer Noise Impact Module from Fig. 2. The L_{AE} noise at the 80 dB level are shown in Fig. 15 c and d, overlaid at KSMO for demonstration.

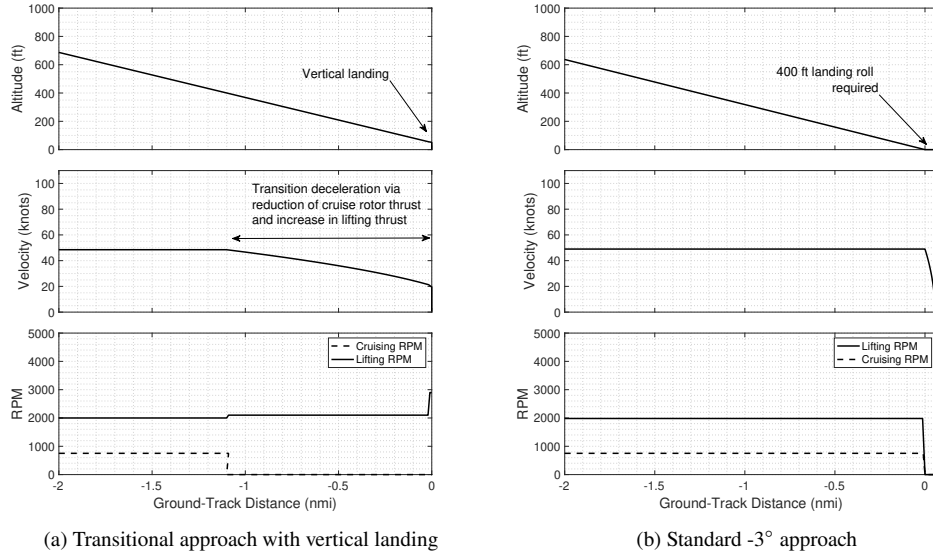
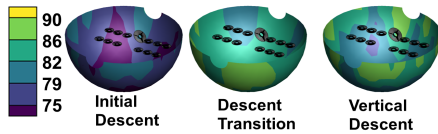
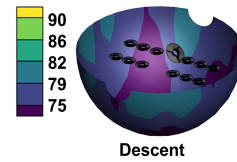


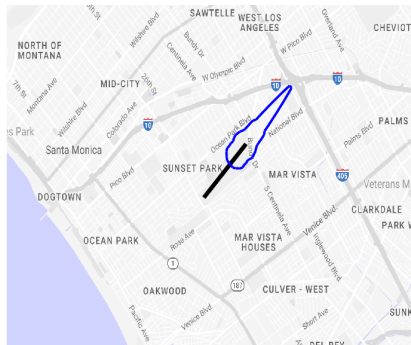
Fig. 14 Example modeled approach procedures for a 2 passenger LPC-VTOL aircraft



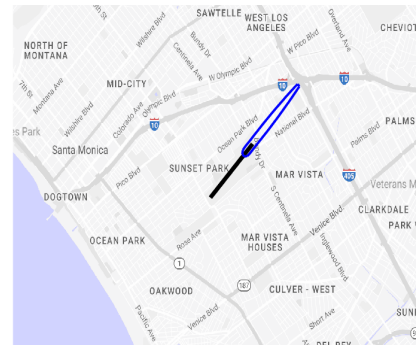
(a) A-Weighted OASPL (dBA) noise hemispheres for the transitional approach with vertical landing



(b) A-Weighted OASPL (dBA) noise hemispheres for the standard -3° approach



(c) 80 dB L_{AE} contour for the transitional approach with vertical landing



(d) 80 dB L_{AE} contour for the standard -3° approach

Fig. 15 Modeled noise hemispheres and L_{AE} (dB) contours overlaid at KSMO of example approach procedures for a 2 passenger LPC-VTOL aircraft

The noise contour for the standard continuous descent approach occupies a significantly smaller area of compared to the transitional approach with a vertical landing, as can be seen in Fig. 15. The standard approach generates a narrow contour of consistent width that continues until the landing roll. In contrast, the transitional approach with

a vertical landing is cone-shaped, growing wider as the vehicle transitions and becomes loudest during the vertical landing segment when the lifting rotors are operating at their highest RPM in the procedure. These results suggest the noise of the LPC-VTOL is very sensitive to propeller RPM rather than flight profile. Although the standard approach holds a high velocity of 48 kts below 400 ft, its contour shows little changes along the ground track distance because its propeller mode remains constant. Conversely, changes in propeller RPM for the lift and cruise rotors are clearly observable with the lifting propellers in vertical landing mode making up the loudest increase in noise. These results indicate the noise contour for a LPC-VTOL approach is primarily dependent of rotor RPM, especially during periods of vertical or transitional flight. The need for a runway, however, should be considered when evaluating the feasibility of conventional approaches for the LPC-VTOL.

VI. Community Noise Modeling Demonstration of a Tilt-Rotor VTOL Vehicle

In this section, example departure and arrival flight operations and resulting community noise characteristics of a representative 4 passenger Tilt-Rotor VTOL vehicle is presented.

A. Vehicle Characteristics

The Tilt-Rotor VTOL vehicle is assumed to operate with rotating rotors capable of providing thrust in the horizontal direction, vertical direction, or at an arbitrary angle of attack denoted by α , depending on the configuration setting. The x-direction and y-direction thrust per rotor, denoted by T_x and T_y , respectively are defined as the x and y components of the thrust vector per rotor, T , illustrated in Fig. 16. T_x and T_y are used to construct the flight profile according to eq.1 and 2 as described in section III.A. The Tilt-Rotor VTOL vehicle is assumed to remain level during all modes of flight.

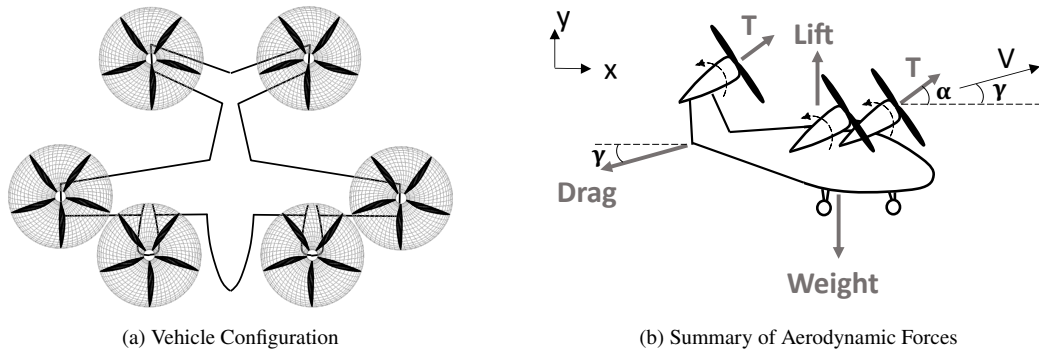


Fig. 16 Vehicle Summary for Tilt-Rotor VTOL

A description of key vehicle properties used to model the flight performance characteristics, rotor blade geometry, and noise are described in Table 5, with aircraft characteristics and known rotor geometry used obtained from [17]. The takeoff and cruise operating points used in the rotor design, including the takeoff thrust and cruise thrust per lifting and cruising rotor, were determined as described in section III.A based on the weight and design cruise speed, respectively. The vertical takeoff thrust magnitude is assumed to be 1.3 times the vehicle weight while the design cruise thrust speed was obtained from the drag at a 152 knots shown Table 3. These conditions were used to determine the rotor geometry as discussed in section III.B.

Table 5 Tilt-Rotor VTOL vehicle properties, referenced from [17], used for example noise analyses

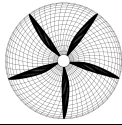
| | | |
|---|---------------------------------------|-------|
| Aircraft Characteristics | Weight (lbs) | 4000 |
| | Span (ft) | 35 |
| | Aspect Ratio | 11.4 |
| | Range (nmi) | 130.3 |
| | Number of Passengers | 4 |
| Known Rotor Geometry | Rotor Diameter (ft) | 9.5 |
| | Number of Rotors | 6 |
| | Number of Blades per Rotor | 5 |
| | Hub Percent of Rotor Diameter (%) | 10 |
| Takeoff and Cruise Operating Points used in Rotor Design | Takeoff Distance (ft) | 0 |
| | Design Takeoff Thrust per Rotor (lb)* | 350 |
| | Design Takeoff Speed (knots)** | 38 |
| | Design Cruise Thrust per Rotor (lb)* | 57 |
| | Design Cruise Speed (knots)* | 152 |

*Determined from desired takeoff and cruise performance

**Value assumed from Blown-Flap STOL vehicle example for rotor sizing

To obtain the rotor geometry per blade section needed for the noise analysis, a rotor was designed with the methodology described in section III.B for a variable pitch rotor. Following the same methodology as the Blown-Flap STOL rotor, a preliminary design point was obtained from the design takeoff and cruise conditions. In contrast with the STOL vehicle, the Tilt-Rotor VTOL rotor was uniquely required to perform a quiet hover and a powered transition. The Tilt-Rotor VTOL midpoint thrust was shifted towards the low thrust condition to optimize the efficiency at higher speeds while lowering noise. The rotor diameter was minimized to lower operating rotor RPM and consequently lower noise M_{tip} to 0.379, as well as during the takeoff and cruise segments. This results in a maximum RPM of 800 with a design condition for transition flight. A summary of the rotor properties is given in Table 6.

Table 6 Tilt-Rotor VTOL rotor properties used for example noise analyses

| | |
|--|--|
| Design Condition | Transition |
| Thrust per rotor at Design Condition (N) | 1100 |
| Velocity at Design Condition (m/s) | 45 |
| Power per rotor at Design Condition (kW) | 55.4 |
| RPM at Design Condition | 800 |
| M_{tip} at Design Condition | 0.379 |
| Max RPM | 800 |
| Rotor characteristics | Variable pitch |
| Rotor image |  |

B. Tilt-Rotor VTOL Vertical Takeoff and Acceleration Climb at 100% Power versus 90% Power

Given the vehicle and rotor properties from Tables 5 and 6, noise analysis was performed on example departure and arrival procedures to demonstrate the methodology outlined in section III. The example departure operation definition for this vehicle is a 100% power departure 800 RPM, consisting of a vertical takeoff until 100 ft. Then, the vehicle

climbs at 15 degrees at maximum RPM until it reaches a horizontal velocity equal to a cruise speed of 140 knots. During this segment, the rotors transition from a lifting orientation facing to a forward facing orientation. Once the cruise speed is reached, the vehicle continues to climb at 15 degrees at the cruise speed. A second departure procedure was modeled with the same parameters, but conducted at 90% the maximum power. For both procedures, RPM is held constant at 800 RPM and required thrust is controlled by changing blade pitch.

Given the inputs described above noise source hemispheres were modeled using the source noise module along the flight trajectory, as shown in Fig. 17 a and b. In both profiles, three noise hemispheres were used to represent the vertical takeoff, transition, and climb-out segments. These noise hemispheres were propagated to the ground in the Observer Noise Impact Module from Fig. 2. The L_{AE} noise at the 70 dB level are shown in Fig. 18 c and d, overlaid at KSMO for demonstration.

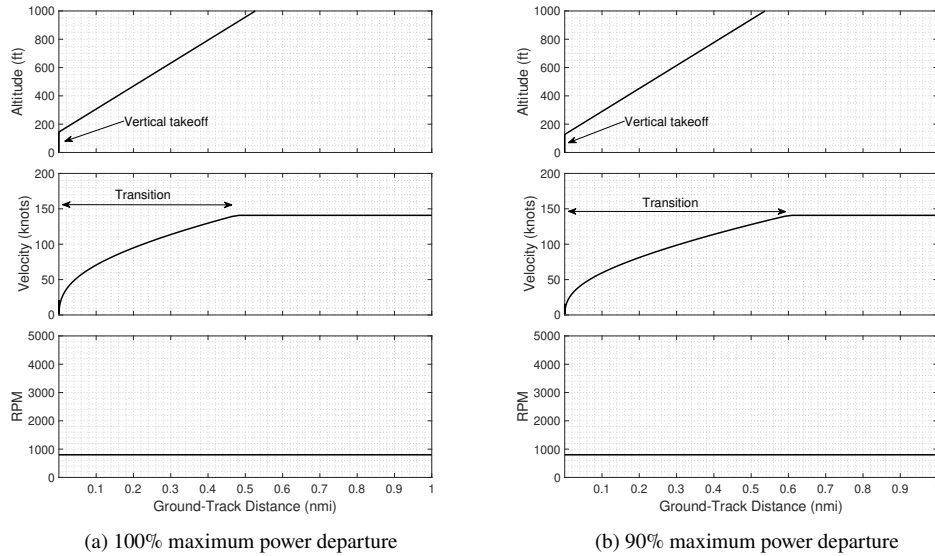


Fig. 17 Example modeled departure procedures for a 4 passenger Tilt-Rotor VTOL aircraft



(a) A-Weighted OASPL (dBA) noise hemispheres for a 100% maximum power departure (b) A-Weighted OASPL (dBA) noise hemispheres for a 90% maximum power departure

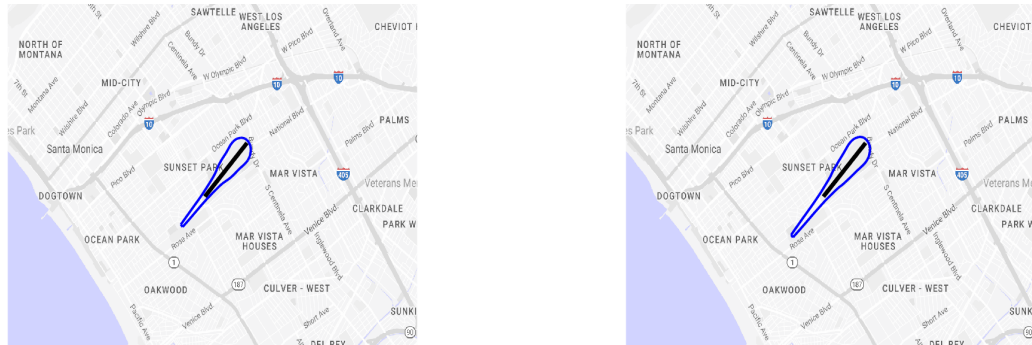


Fig. 18 Modeled noise hemispheres and L_{AE} (dB) contours overlaid at KSMO of example departure procedures for a 4 passenger Tilt-Rotor VTOL aircraft

The departure noise contour for both profiles, shown in Fig. 18, are cone shaped with a wide, round end at the location of the vertical takeoff and a narrowing tip following the vehicle's transition and climb-out flight segments. Compared to climb-out, these segments require the most power and have the least atmospheric attenuation due to their low altitude. The 90% maximum power departure features a narrowed and elongated contour when compared to that of the full power case. Although the power reduction resulted in a quieter vertical takeoff and transition segment, the increased time spent at a lower altitude increased the contour area during climb out when compared to the full power case. These results suggest that during departure, rotor conditions and flight profile both impact tilt-rotor VTOL noise contours.

C. Example Noise Analysis of a Tilt-Rotor VTOL Transitional Approach with Vertical Landing Compared to a Standard -3° Continuous Descent Approach

The Tilt-Rotor VTOL arrival examples compare a transitional approach on a -3° descent with a vertical landing procedure to a standard -3° continuous descent approach and are presented in Fig. 19 a and b. The vertical landing procedure is achieved with a decelerating transitional segment from 100 knots in which the rotors transition from the horizontal, cruise condition to an α of 86° from the horizontal, which provides the necessary vertical thrust at 800 RPM to maintain the vehicles weight. Once the vehicle airspeed reaches 20 knots, the rotors adjust to fully vertical orientation to perform a vertical descent directly over the runway. This operation is compared to a standard -3° continuous descent approach, in which the Tilt-Rotor VTOL maintains a 100 knot velocity while descending without changing the configuration of the rotors and at the same RPM of 800. This procedure requires 1100 ft for the landing roll distance due to the high landing speed which should be considered when evaluating the feasibility of this procedure.

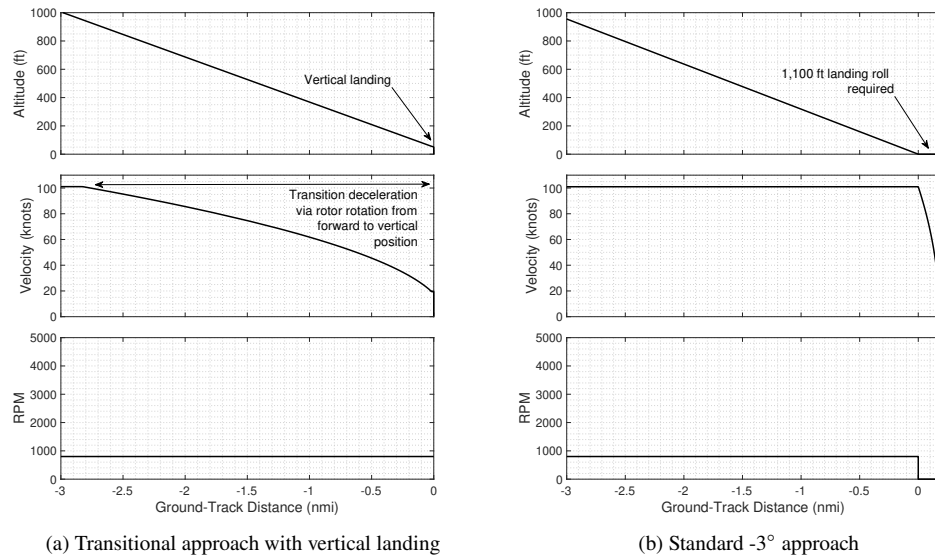
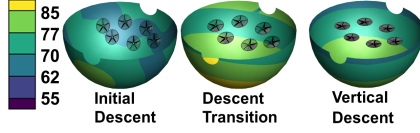


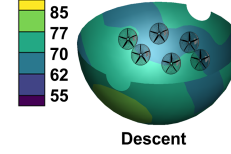
Fig. 19 Example modeled approach procedures for a 4 passenger Tilt-Rotor VTOL aircraft

Given the inputs described above, noise source hemispheres were modeled using the source noise module along the flight trajectory, as shown in Fig. 21 a and b. These noise hemispheres were propagated to the ground in the Observer Noise Impact Module from Fig. 2. The L_{AE} noise at the 75 dB levels are shown in Fig. 21 c and d, overlaid at KSMO for demonstration.

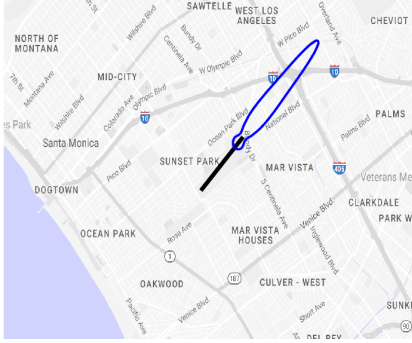
As seen in Fig. 21 the noise contour of the transitional approach was significantly larger in width and length compared to that of the standard approach. The majority of this vertical landing noise occurred during the transitional approach segment. Compared to the standard approach, at similar altitude points, the transitional approach was slower and louder. This suggests tilt-rotor VTOL noise is more sensitive to rotor conditions during periods of vertical or transitional flight than it is to flight path variation.



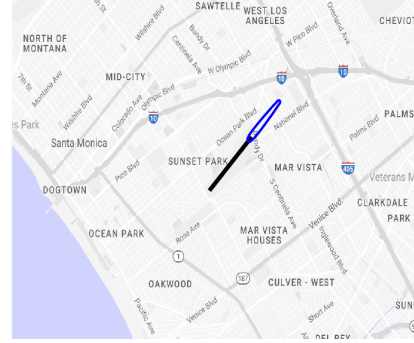
(a) A-Weighted OASPL (dBA) noise hemispheres for a transitional approach with vertical landing



(b) A-Weighted OASPL (dBA) noise hemispheres for a standard -3° approach



(c) 75 dB L_{AE} contour for a transitional approach with vertical landing



(d) 75 dB L_{AE} Contour for a standard -3° approach

Fig. 21 Modeled noise hemispheres and L_{AE} (dB) contours overlaid at KSMO of example approach procedures for a 4 passenger Tilt-Rotor VTOL aircraft

VII. Conclusion

The methodology presented in this paper presents a preliminary capability to output community noise contours produced by various types of AAM vehicles operating in various departure and arrival procedures. The methodology consists of a flight profile generation module, an aircraft performance module to both assess both aerodynamic forces and rotor performance along a flight segment, including the design of representative rotor blade geometries, a source noise module to obtain rotor noise, airframe noise, and preliminary interaction noise sources, and an observer noise impact module to propagate the source noise to the ground. In several examples of different AAM vehicles, the community noise levels over KSMO are shown to have a high sensitivity to different AAM operations and rotor RPM, depending on the vehicle and rotor geometry. From these results, additional types of procedures, rotor designs, and vehicles could be analyzed. Future iterations of the framework and vehicle noise analysis will feature additional interaction noise sources, such as rotor-wake interaction noise, fuselage-wake interaction noise, and blade vortex interaction noise. In addition, future flight procedures could be assessed and tailored to minimize community noise exposure.

Acknowledgments

This work was sponsored by the Federal Aviation Administration (FAA) under ASCENT Center of Excellence Project 84. Opinions, interpretations, conclusions, and recommendations are those of the authors and are not necessarily endorsed by the United States Government. The authors would like to acknowledge the support of Susumu Shirayama of the FAA Office of Environment and Energy.

References

- [1] Antcliff, K., and *et al.*, "Regional Air Mobility: Leveraging Our National Investments to Energize the American Travel Experience," Tech. Rep. NASA-WP-20210014033, 2021.
- [2] Rizzi, S. A., and *et. al.*, "Urban Air Mobility Noise: Current Practice, Gaps, and Recommendations," NASA TP-2020-5007433, 2020.

- [3] Thomas, J., and Hansman, R. J., "Framework for Analyzing Aircraft Community Noise Impacts of Advanced Operational Flight Procedures," *Journal of Aircraft*, Vol. 54, No. 4, 2019. <https://doi.org/10.2514/1.C035100>.
- [4] Lopes, L. V., and Burley, C. L., "ANOPP2 User's Manual: Version 1.2," NASA TM 2016-219342, 2016.
- [5] Courtin, C., and *et al*, "A Performance Comparison of eSTOL and eVTOL Aircraft," AIAA 2021-3220, AIAA Aviation 2021 Forum, 2021.
- [6] Weick, F. E., *Aircraft Propeller Design*, McGraw-Hill Book Co, 1930.
- [7] Vesa, J., "Design of an Anechoic Chamber for Aeroacoustic Testing and Analysis of Large UAS Propellers," Master's thesis, Mississippi State University Masters Thesis, 2020. URL <https://scholarsjunction.msstate.edu/td/1307>.
- [8] Krishnamurthy, S., Tuttle, B. C., and Rizzi, S., "A Synthesis Plug-in for Steady and Unsteady Loading and Thickness Noise Auralization," AIAA AVIATION 2020 FORUM, 2020.
- [9] Brooks, T. F., Pope, D. S., and Marcolini, M. A., "Airfoil Self-Noise and Prediction," Tech. Rep. NASA-RP-1218, Hampton, Virginia, 1989.
- [10] Fink, M., "Airframe Noise Prediction Method," Tech. Rep. FAA-FRD-77-29, 1977.
- [11] Guo, Y., "An Improved Landing Gear Noise Prediction Scheme," Tech. Rep. NASA/CR-NAS1-NNL04AA11B, The Boeing Company, Huntington Beach, CA, 2006.
- [12] Guo, Y., "Aircraft Flap Side Edge Noise Modeling and Prediction," 32nd AIAA Aeroacoustics Conference, 2011.
- [13] Courtin, C., Hansman, R. J., and Drela, M., "Flight Test Results of a Subscale Super-STOL Aircraft," AIAA 2020-0977, AIAA Scitech 2020 Forum, 2020.
- [14] Yeung, N., and *et al*, "Component Noise Modeling for Distributed Propulsion Blown-Flap STOL Vehicle Flight Procedures," AIAA 2022-3508, AIAA Aviation, 2022.
- [15] Agrawal, D., and *et al*, "Wind Tunnel Testing of a Blown Flap Wing," AIAA 2019-3170, AIAA Aviation, 2019.
- [16] Bacchini, A., and Cestino, E., "Electric VTOL Configurations Comparison," *Aerospace*, Vol. 6, No. 3, 2019. <https://doi.org/10.3390/aerospace6030026>.
- [17] Pascioni, K. A., Watts, M. E., Houston, M., Lind, A., Stephenson, J. H., and Bain, J., "Acoustic Flight Test of the Joby Aviation Advanced Air Mobility Prototype Vehicle," *28th AIAA/CEAS Aeroacoustics 2022 Conference*, Southampton, UK, 2022. <https://doi.org/10.2514/6.2022-3036>.